BBr_3 DIFFUSION: PROCESS OPTIMIZATION FOR HIGH-QUALITY EMITTERS WITH INDUSTRIAL CYCLE TIMES

E. Lohmüller[1], M. Glatz[1], S. Lohmüller[1], U. Belledin[1], S. Mack[1], T. Fellmeth[1], R.C.G. Naber[2], A. Wolf[1]
[1]Fraunhofer Institute for Solar Energy Systems ISE, Heidenhofstrasse 2, 79110 Freiburg, Germany
[2]Tempress Systems, Radeweg 31, 8171MD, Vaassen, The Netherlands
Phone: +49 761 - 4588 5701; e-mail: elmar.lohmueller@ise.fraunhofer.de

ABSTRACT: We demonstrate tube furnace BBr_3 diffusion processes for the formation of high-quality homogeneous boron emitters with industrial cycle times of around 2 hours. They feature emitter dark saturation current densities as low as 17 fA/cm² for textured surfaces at a sheet resistance of about 150 Ω/sq. In order to achieve the respective doping profiles with a maximum charge carrier concentration slightly above 10^{19} cm^{-3} and profile depths of about 800 nm, we optimize the atmospheric pressure BBr_3 diffusion such that we make use of an increased maximum temperature (below 1000°C) that yields accelerated diffusion of boron atoms. In addition, careful parameter adjustment assures that the total boron doping dose in the silicon is maintained, despite the temperature increase. This optimization shows a great potential in reducing cycle times without compromising the quality of the formed boron emitters and their respective doping profiles.
Keywords: BBr_3 diffusion, boron emitter, process optimization, recombination, cycle time reduction

1 INTRODUCTION

The emitter dark saturation current density j_{0e} for the passivated front side boron emitter in n-type silicon solar cells can be drastically reduced by lowering the maximum doping concentration N_{max} at or close to the silicon surface [1–7]. For the formation of boron emitters, the state-of-the-art technology is a tube furnace diffusion using boron tribromide (BBr_3) as liquid dopant precursor [8]. In order to achieve charge carrier recombination at an sufficiently low level for screen-printed and fired silver-aluminum contacts while ensuring low specific contact resistance ρ_C, it is a straight forward approach to increase the profile depth d_{prof} when lowering N_{max} [9,10].

Several adaptations within the BBr_3 diffusion process can be considered to lower N_{max} and to increase d_{prof} in the resulting doping profile. A very promising and industrially relevant approach that fulfills both points is the usage of a post-oxidation step in oxygen (O_2) ambient that is incorporated into the diffusion process [4,11]. By post-oxidation, segregation of boron into the growing silicon dioxide (SiO_2) layer on the silicon surface [12] and oxidation-enhanced diffusion of boron [13] lead to a decrease in N_{max} and redistribution of boron dopants. Despite reduction in N_{max}, low ρ_C in the range of a few $m\Omega cm^2$ is state-of-the-art for commercial screen-printed and fired silver-aluminum (Ag-Al) contacts [3,6,14]. As exemplified in Ref. [6], $\rho_C \approx 3$ $m\Omega cm^2$ is found for screen-printed and fired Ag-Al contact fingers for quite low $N_{max} = 1.8 \cdot 10^{19}$ cm^{-3}.

Cycle times (including load/unload) of tube furnace diffusion processes of up to 3.5 hours are currently quite common in the industry in order to produce high-quality emitters for high-efficiency n-type devices, such as e.g. solar cells with tunnel oxide passivated contacts (TOPCon) [15].

In this paper, we perform process optimizations for atmospheric pressure BBr_3 diffusion executed in an industrial tube furnace from Tempress Systems ("SPECTRUM MULTI PURPOSE 5 stack furnace"). We aim at forming boron emitters that feature very low j_{0e} on alkaline textured and passivated surfaces at emitter sheet resistances in the range of 150 Ω/sq. We demonstrate the formation of high-quality boron emitters using single BBr_3 diffusion processes with industrial cycle times of around 2 hours.

2 APPROACH

We perform three optimization runs A - C, each with several BBr_3 diffusion processes to optimize the recipes, targeting an emitter sheet resistance $R_{sh} \approx 150$ Ω/sq with a doping profile featuring a low N_{max} in the range of 10^{19} cm^{-3} and a large d_{prof} close to 1 µm. Therefore, we continue the developments from Ref. [4] and start with industrially common cycle times t_c (including load/unload) in the range of 3.5 hours. Then, we considerably reduce t_c to slightly above 2 hours.

In total, we examine eleven different BBr_3 diffusion processes. Their allocation to the three runs is as follows:

- Run A (Diff1 - Diff5)
  The maximum temperature of the diffusion processes is $T_{max} = T_1$. Variation of drive-in time $t_{dr\text{-}in}$ and post-oxidation time t_{po} resulting in 135 min ≤ t_c ≤ 205 min.
- Run B (Diff6 - Diff8)
  Increase of T_{max} by 40K (T_{max} below 1000°C) starting from Diff1 and variation in $t_{dr\text{-}in}$ resulting in 129 min ≤ t_c ≤ 149 min.
- Run C (Diff9 - Diff11)
  T_{max} as in B, further optimization and careful parameter adjustment of the diffusion process with 133 min ≤ t_c ≤ 143 min.

3 EXPERIMENTAL PROCEDURE AND DIFFUSION BOAT LOADING

For the optimization of the atmospheric pressure BBr_3 diffusion, we apply the processes and characterization steps as shown in Fig. 1. We use *p*-type Czochralski-grown silicon (Cz-Si) wafers with saw damage etched (SDE) surfaces. Any existing thermal donors have been previously dissolved during a high-temperature step [16].

Prior to BBr_3 diffusion, the sheet resistance of the silicon base is measured and the surfaces are cleaned by wet-chemical processing in hydrofluoric acid (HF). Then, the eleven BBr_3 diffusion processes Diff1 - Diff11, as described in chapter 2, are carried out. The boat setup with a wafer-to-wafer distance of 4.76 mm (full pitch) is depicted in Fig. 2. The boat holds 300 wafers in total for

full pitch single-slot loading. We evenly distribute packages with 15 samples each at five positions P1 - P5 over the entire boat. This provides information about the properties and general applicability of the respective BBr_3 diffusion process for full boat loadings. Position P1 is located at the gas inlet; position P5 is at the furnace door. The neighboring wafers to the p-type Cz-Si characterization samples are virgin dummy wafers with bare silicon surface. Additional dummy wafers covered with borosilicate glass/silicon dioxide (BSG/SiO_2) surround these wafers.

After BBr_3 diffusion and wet-chemical etching of the BSG/SiO_2 layer stack in HF, the total sheet resistance, consisting of contributions from the base and the boron doping, is measured. Then, the sheet resistance R_{sh} of the boron doping is calculated from the measurements before and after diffusion over the wafer surface for all five boat positions P1 - P5 (details regarding the measurement and calculation can be found in Ref. [4]).

Finally, the charge carrier concentration profile $N(d)$ for the sample at position P1 is determined by the electrochemical capacitance-voltage (ECV) technique [17]. The surface area factor is adjusted such that the R_{sh} of the doping profile matches the R_{sh} measured inductively at the ECV measurement spot.

For some of the diffusion processes, j_{0e} is examined on alkaline textured, Al_2O_3/SiN_X-passivated and fired n-type Cz-Si lifetime samples with base resistivities

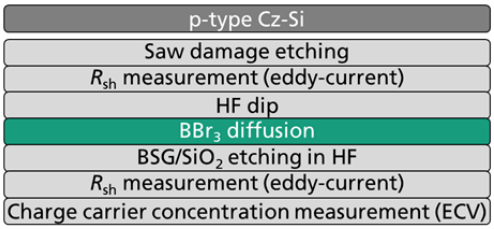

Figure 1: Schematic process sequence used for the BBr_3 diffusion process optimizations.

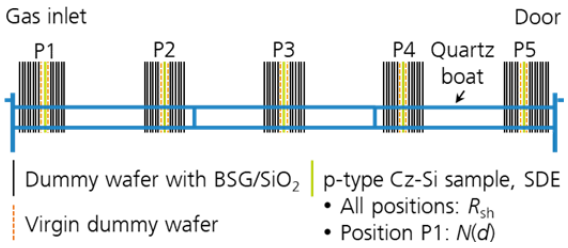

Figure 2: Schematic illustration of the wafer arrangement in the quartz boat for the characterization of the BBr_3 diffusion processes (not to scale). The boat positions are indicated by P1 - P5.

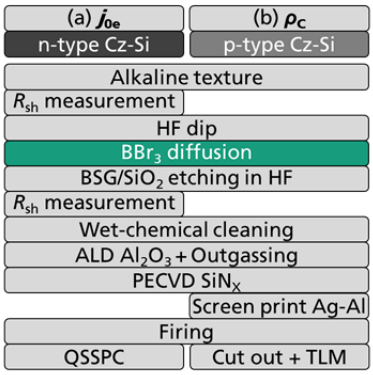

Figure 3: Schematic process sequences for the examination of (a) j_{0e} and (b) ρ_C for some of the BBr_3 diffusion processes (ALD: atomic layer deposition, PECVD: plasma-enhanced chemical vapor deposition, QSSPC: quasi-steady-state photoconductance, TLM: transmission line model).

between 3 Ωcm < ρ_b < 8 Ωcm (after thermal donor annihilation [16]); see Fig. 3(a). The symmetrically passivated j_{0e} samples are measured by QSSPC after firing. Then, the evaluation of the j_{0e} values is performed according to the procedure from Kimmerle et al. [18].

Also, for the emitters Diff1 - Diff4, ρ_C for a commercially available Ag-Al screen-printing paste is determined. For Diff1 and Diff2, TLM samples according to Fig. 3(b) are examined. The Ag-Al fingers are printed with a nominal screen opening of 40 µm on textured and Al_2O_3/SiN_X-passivated samples. After firing, the samples are cut in 1 cm-wide strips, TLM measurements are performed and ρ_C is evaluated. For Diff3 and Diff4, the TLM measurements are performed after cutting the strips out of fully processed TOPCon solar cells. Here, the Ag-Al fingers are printed with a nominal screen opening of 24 µm.

The corresponding samples for both, j_{0e} and ρ_C, are processed together in separate diffusion runs being located in the boat range of position P1.

4 BBr_3 DIFFUSION OPTIMIZATION RUNS

4.1 Run A

Some properties of the five different BBr_3 diffusion processes Diff1 - Diff5 are summarized in Table I. The cycle time t_c (including load/unload) increases from t_c = 135 min (Diff1) over t_c = 175 min (Diff2) to t_c = 205 min (Diff3 - Diff5). The longer t_c results from increased t_{po}. For Diff3 - Diff5, t_c = 205 min stays constant, however, the shares of $t_{dr\text{-}in}$ and t_{po} are changed.

Fig. 4 illustrates the mean sheet resistances R_{sh} over the wafer at the five different boat positions P1 - P5 that range between R_{sh} ≈ 100 Ω/sq for Diff1 and R_{sh} ≈ 160 Ω/sq

Table I: Summary of parameters of the investigated BBr_3 diffusion processes of optimization run A. In the cycle time t_c, the loading and unloading of the boat is included with 6.5 min each. The mean R_{sh} from all samples at the five positions over the boat P1 - P5 are given as $R_{sh,mean,boat}$. The standard deviation of this value gives the homogeneity over the boat. The profile depth d_{prof} is extracted at $N = 10^{17}$ cm^{-3}.

BBr_3 diffusion	**T_{max}**	**t_c** (min)	**$R_{sh,mean,boat}$** (Ω/sq)	**N_{max}** (10^{19} cm^{-3})	**d_{prof}** (nm)	**j_{0e}** (fA/cm²)	**ρ_C** (mΩcm²)
Diff1		135	106 ± 3	2.9 ± 0.3	640 ± 64	31 ± 1	2.0 ± 0.3
Diff2		175	112 ± 2	1.9 ± 0.2	800 ± 80	27 ± 3	2.2 ± 0.6
Diff3	T_1	205	124 ± 1	1.4 ± 0.1	910 ± 91	22 ± 1	2.6 ± 1.1
Diff4		205	154 ± 5	1.1 ± 0.1	860 ± 86	15 ± 3	3.8 ± 1.4
Diff5		205	151 ± 6	1.2 ± 0.1	860 ± 86	-	-

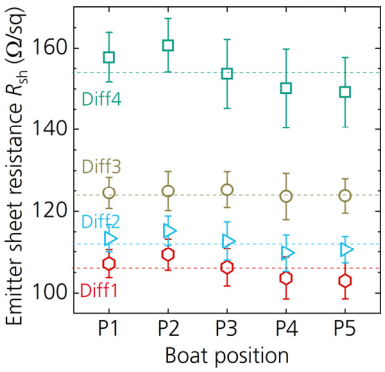

Figure 4: Eddy-current measured mean R_{sh} for the SDE samples at the five different boat positions P1 - P5 as illustrated in Fig. 2. The error bars indicate the standard deviation of R_{sh} over the wafer according to Ref. [4]. The dashed lines are guides to the eye.

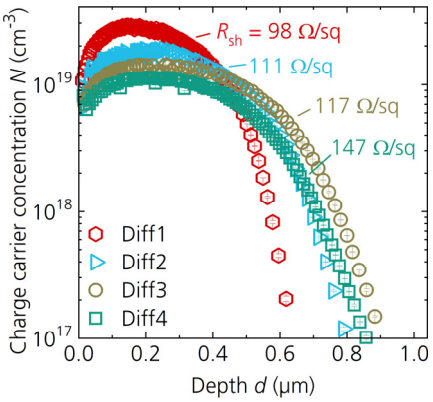

Figure 5: Charge carrier concentration profiles measured by ECV on SDE surface for the samples at position P1. The measurements are performed at the samples' center. The given sheet resistances R_{sh} are measured by eddy-current near the ECV spot.

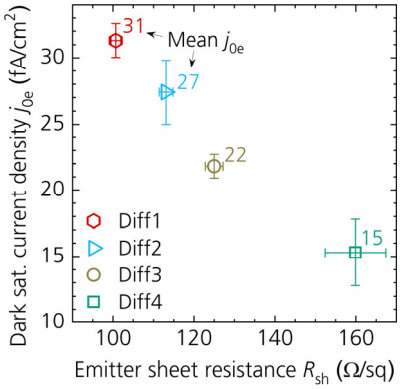

Figure 6: Emitter dark saturation current density j_{0e} versus emitter sheet resistance R_{sh} on textured surfaces. The j_{0e} is examined on symmetrically Al_2O_3/SiN_X-passivated n-type Cz-Si wafers (positioned at P1) after firing.

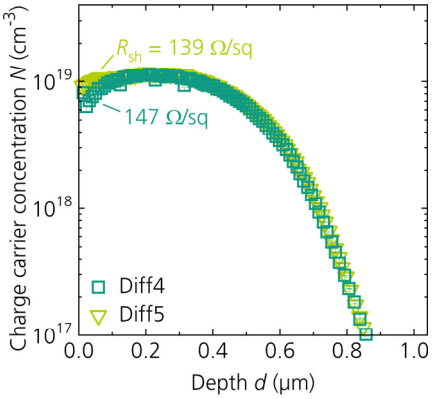

Figure 7: Charge carrier concentration profiles measured by ECV on SDE surface for the samples at position P1.

for Diff4 determined on SDE surfaces. The mean wafer uniformity in R_{sh} is: 4.0% (Diff1), 3.5% (Diff2), 3.7% (Diff3), and 5.1% (Diff4). The standard deviation of $R_{sh,mean,boat}$ is quite low with values well below 4%. Note that all five heating zones of the furnace have the same temperature throughout this work; no temperature tilting has been implemented yet. Thus, the homogeneity of R_{sh} over the single wafers as well as over the entire boat is already very satisfactory.

Fig. 5 shows the charge carrier concentration profiles $N(d)$ measured by ECV. The maximum charge carrier concentration N_{max} decreases steadily from $N_{max} = (2.9 \pm 0.3) \cdot 10^{19}$ cm^{-3} for Diff1 to $N_{max} = (1.1 \pm 0.1) \cdot 10^{19}$ cm^{-3} for Diff4. The profile depth increases from $d_{prof} \approx 600$ nm up to $d_{prof} \approx 900$ nm.

The j_{0e} for diffusion Diff1 to Diff4 is shown in Fig. 6. Obviously, the optimization leads to significantly lower j_{0e} values down to $j_{0e} = (15 \pm 3)$ fA/cm² at $R_{sh} \approx 160$ Ω/sq measured on textured surface.

Using a commercially-available Ag-Al screen-printing paste, these lowly-doped emitters can be electrically contacted with low specific contact resistances between 2 mΩcm² ≤ ρ_C ≤ 4 mΩcm²; see Table I.

Diffusion process Diff4 has already been implemented into large-area (M2 wafer format) n-type Cz-Si TOPCon solar cells using screen-printed and fired contacts on both sides. The most efficient cell achieves an energy conversion efficiency of 22.95% (measured by Fraunhofer ISE CalLab PVCells) [19].

As seen from Fig. 5, the doping density $N(d)$ decreases quite strongly towards the surface for all four profiles. This is due to the fact that the solubility of boron is higher in SiO_2 than in silicon (i.e. the segregation coefficient of boron is lower than 1) [12]. For state-of-the-art metallization, i.e. screen-printed and fired Ag-Al paste, this $N(d)$ decrease towards the surface is currently not particularly relevant for achieving low ρ_C. Since the penetration of metal crystallites into the emitter is significantly deeper with depths of up to several µm [9,20–23], more highly doped areas contribute to ρ_C [9]. However, for pure silver pastes, the crystallites are usually significantly smaller (see e.g. Refs. [24–26] for silver contacts on phosphorus-doped surfaces). Hence, this surface depletion could then play a role in low-resistance electrical contacting. For such a scenario, we adapt Diff4 to decrease the surface depletion to a minimum. The successful adaption is shown in Fig. 7. While the deep parts of the profiles, i.e. for $d > 150$ nm, are identical for Diff4 and Diff5, the surface depletion is considerably reduced for Diff5. We estimate the influence of the decreased surface depletion on j_{0e} to be very small. Whether it is beneficial for electrical contacting with pure silver pastes remains to be investigated.

The BBr_3 diffusion variations in run A show very promising results and the used cycle times of about 3.5 hours are quite common in the industry for mass production of high-efficiency cells.

Table II: Summary of parameters from the indicated BBr_3 diffusion processes of optimization run B.

BBr_3 diffusion	T_{max}	t_c (min)	$R_{sh,mean,boat}$ (Ω/sq)	N_{max} (10^{19} cm^{-3})	d_{prof} (nm)	j_{0e} (fA/cm²)	ρ_C (mΩcm²)
Diff6		149	61 ± 2	3.2 ± 0.3	1000 ± 100	-	-
Diff7	T_1 + 40K	139	72 ± 1	2.8 ± 0.3	920 ± 92	-	-
Diff8		129	90 ± 1	2.3 ± 0.2	850 ± 85	-	-

Table III: Summary of parameters from the indicated BBr_3 diffusion processes of optimization run C.

BBr_3 diffusion	T_{max}	t_c (min)	$R_{sh,mean,boat}$ (Ω/sq)	N_{max} (10^{19} cm^{-3})	d_{prof} (nm)	j_{0e} (fA/cm²)	ρ_C (mΩcm²)
Diff9		143	133 ± 4	1.6 ± 0.2	760 ± 76	-	-
Diff10	T_1 + 40K	138	144 ± 6	1.5 ± 0.2	780 ± 78	17 ± 2	-
Diff11		133	165 ± 8	1.3 ± 0.1	820 ± 82	-	-

4.2 Run B

In order to realize similar deep and lowly-doped emitters as for Diff2 - Diff4, but to shorten the cycle time t_c significantly, we carry out three adjustments starting from Diff1; see Table II. For Diff6, we increase the maximum temperature to $T_{max} = T_1 + 40K$ without further changes (T_{max} is below 1000°C). For Diff7 and Diff8, we shorten $t_{dr\text{-}in}$ by 10 min and 20 min, respectively.

The R_{sh} for the adjusted BBr_3 diffusion processes Diff6 - Diff8 ranges between 60 Ω/sq ≤ R_{sh} ≤ 90 Ω/sq; see Fig. 8. We could decrease t_c quite considerably to 129 min ≤ t_c ≤ 149 min. While doing so, the profile depth d_{prof} increases even slightly; compare Fig. 9 with Fig. 5. However, the maximum doping concentration N_{max} is still above $2 \cdot 10^{19}$ cm^{-3} and thus higher as for Diff2 - Diff4 from optimization run A. Due to the higher T_{max}, more boron can be dissolved in the silicon, which then results in a higher N_{max} for Diff6 - Diff8. Thus, j_{0e} is expected to be somewhat higher for these emitters.

4.3 Run C

In order to decrease N_{max} to below $2 \cdot 10^{19}$ cm^{-3}, thus being at a comparable level to Diff2 - Diff5 from optimization run A, we improve the BBr_3 diffusion even further. We use the same maximum temperature as in run B, i.e. $T_{max} = T_1 + 40K$; see Table III. We apply careful parameter adjustments and keep t_c within 133 min ≤ t_c ≤ 143 min in order to be similarly short as in optimization run B.

The R_{sh} for the adjusted BBr_3 diffusion processes Diff9 - Diff11 ranges between 130 Ω/sq ≤ R_{sh} ≤ 170 Ω/sq determined on SDE surfaces; see Fig. 10. The mean wafer uniformity in R_{sh} is: 5.5% (Diff9), 6.5% (Diff10), and 7.5% (Diff11). The standard deviation of $R_{sh,mean,boat}$ is again quite low with values below 5%.

With $d_{prof} \approx$ 800 nm, we keep d_{prof} comparably deep as for the optimization runs A and B; see Fig. 11. We have managed to decrease N_{max} to $N_{max} \approx 1.5 \cdot 10^{19}$ cm^{-3} in comparison to the doping profiles from run B with $2.3 \cdot 10^{19}$ cm^{-3} ≤ N_{max} ≤ $3.2 \cdot 10^{19}$ cm^{-3}.

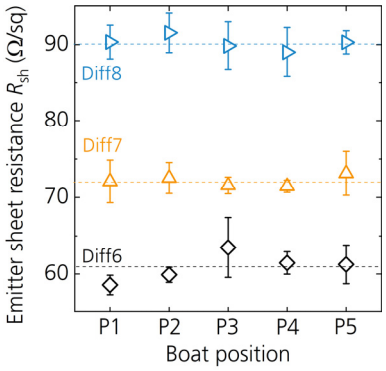

Figure 8: Eddy-current measured mean R_{sh} for the SDE samples at the boat positions P1 - P5.

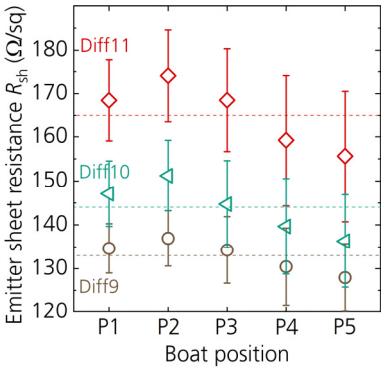

Figure 10: Eddy-current measured mean R_{sh} for the SDE samples at the boat positions P1 - P5.

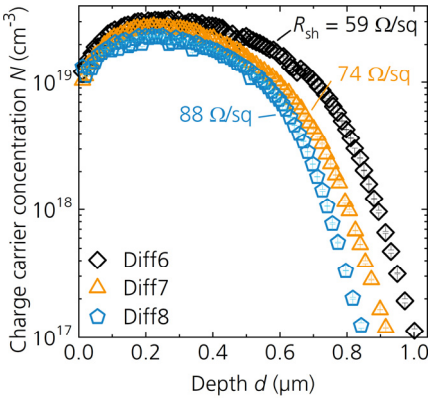

Figure 9: Charge carrier concentration profiles measured by ECV on SDE surface for the samples at position P1.

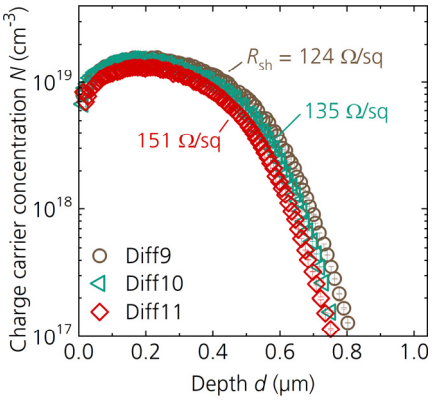

Figure 11: Charge carrier concentration profiles measured by ECV on SDE surface for the samples at position P1.

The j_{0e} for diffusion Diff10 is found to be $j_{0e} = (17 \pm 2)$ fA/cm² at $R_{sh} \approx 150$ Ω/sq on textured surface.

Comparing the results of e.g. Diff10 to Diff3/Diff4, it is seen that the cycle time of the BBr_3 diffusion process is decreased by more than one hour while yielding boron emitters with quite similar properties.

This demonstrates the possibility to form high-quality boron emitters with cycle times of not much more than 2 hours.

5 SUMMARY AND CONCLUSION

The optimization of BBr_3 diffusion processes in three cycles yields high-quality boron emitters with emitter dark saturation current density j_{0e} values on textured and Al_2O_3/SiN_X-passivated surface as low as 17 fA/cm² at an emitter sheet resistance $R_{sh} \approx 150$ Ω/sq.

Being able to decrease the cycle time by more than 1 hour to slightly more than 2 hours offers potential for further cost reduction in mass-production. We achieve this time reduction by increasing the maximum temperature (below 1000°C) and careful process parameter adaptions.

The boron emitters feature charge carrier concentration profiles with a maximum doping concentration $N_{max} \approx 1.5 \cdot 10^{19}$ cm^{-3} and a profile depth $d_{prof} \approx 800$ nm. The homogeneity of R_{sh} over the boat examined by using test samples at five different boat positions is already very satisfactory with a standard deviation below 5%. The low-ohmic electrical contacting of such boron emitters with low N_{max}, when applying a commercially-available screen-printed silver-aluminum paste, is confirmed with specific contact resistances found to be between 2 mΩcm² and 4 mΩcm².

We also show that the surface depletion of the charge carrier concentration can be reduced to a minimum while not changing the rest of the profile. This might be an option to improve low-resistance electrical contacting when applying pure silver contacts.

This work demonstrates the possibility to significantly decrease the cycle times of BBr_3 diffusion processes to slightly above 2 hours while still being able to form high-quality boron emitters. These emitters are therefore extremely suitable for implementation in, e.g., n-type Cz-Si TOPCon solar cells.

ACKNOWLEDGEMENTS

The authors would like to thank all colleagues at the Fraunhofer ISE PV-TEC. Project “RHINO” is supported under the umbrella of SOLAR-ERA.NET Cofund by the German Federal Ministry of Economic Affairs and Energy under contract number 0324224A. SOLAR-ERA.NET is supported by the European Commission within the EU Framework Programme for Research and Innovation “HORIZON 2020” (Cofund ERA-NET Action, N°691664).

REFERENCES

[1] Y. Schiele, S. Joos, G. Hahn et al., "Etch-back of p+ structures for selective boron emitters in n-type c-Si solar cells", *Energy Proced.*, vol. 55, pp. 295–301, 2014.

[2] F. Kiefer, R. Peibst, T. Ohrdes et al., "Emitter recombination current densities of boron emitters with silver/aluminum pastes", *Proc. 40th IEEE PVSC*, Denver, USA, 2014, pp. 2808–2812.

[3] Y. Schiele, G. Hahn, B. Terheiden, "Contacting and recombination analysis of boron emitters via etch-back for advanced n-type Si solar cells", *Proc. 29th EU PVSEC*, Amsterdam, The Netherlands, 2014, pp. 825–829.

[4] S. Werner, E. Lohmüller, U. Belledin et al., "Optimization of BBr_3 diffusion processes for n-type silicon solar cells", *Proc. 31st EU PVSEC*, Hamburg, Germany, 2015, pp. 637–641.

[5] N. Wöhrle, E. Lohmüller, S. Werner et al., "Development, characterization, and modelling of doping profile, contact resistance, and metal spiking in diffused and screen-printed boron emitters", *Proc. 31st EU PVSEC*, Hamburg, Germany, 2015, pp. 495–501.

[6] S. Werner, E. Lohmüller, A. Wolf et al., "Extending the limits of screen-printed metallization of phosphorus- and boron-doped surfaces", *Sol. Energy Mater. Sol. Cells*, vol. 158, pp. 37–42, 2016.

[7] M. Li, F.-J. Ma, I. M. Peters et al., "Numerical simulation of doping process by BBr_3 tube diffusion for industrial n-type silicon wafer solar cells", *IEEE J. Photovoltaics*, vol. 7, no. 3, pp. 755–762, 2017.

[8] ITRPV, 2020, "International Technology Roadmap for Photovoltaic (ITRPV) - Results 2019.

[9] E. Lohmüller, S. Werner, R. Hoenig et al., "Impact of boron doping profiles on the specific contact resistance of screen printed Ag-Al contacts on silicon", *Sol. Energy Mater. Sol. Cells*, vol. 142, pp. 2–11, 2015.

[10] N. Wöhrle, E. Lohmüller, J. Greulich et al., "Towards understanding the characteristics of Ag-Al spiking on boron-doped silicon for solar cells", *Sol. Energy Mater. Sol. Cells*, vol. 146, pp. 72–79, 2016.

[11] J. Libal, R. Petres, T. Buck et al., "N-Type multicrystalline silicon solar cells: BBr_3-diffusion and passivation of p+-diffused silicon surfaces", *Proc. 20th EU PVSEC*, Barcelona, Spain, 2005, pp. 793–796.

[12] A. S. Grove, O. Leistiko, C. T. Sah, "Redistribution of acceptor and donor impurities during thermal oxidation of silicon", *J. Appl. Phys.*, vol. 35, no. 9, pp. 2695–2701, 1964.

[13] K. Taniguchi, K. Kurosawa, M. Kashiwagi, "Oxidation enhanced diffusion of boron and phosphorus in (100) silicon", *J. Electrochem. Soc.*, vol. 127, no. 10, pp. 2243–2248, 1980.

[14] T. Buck, J. Theobald, M. Nejati et al., "Engineering and characterization of metal contacts to p+-doped silicon", *Proc. 29th EU PVSEC*, Amsterdam, The Netherlands, 2014, pp. 401–405.

[15] F. Feldmann, M. Bivour, C. Reichel et al., "Passivated rear contacts for high-efficiency n-type Si solar cells providing high interface passivation quality and excellent transport characteristics", *Sol. Energy Mater. Sol. Cells*, vol. 120, pp. 270–274, 2014.

[16] W. Götz, G. Pensl, W. Zulehner et al., "Thermal donor formation and annihilation at temperatures above 500 °C in Czochralski-grown Si", *J. Appl. Phys.*, vol. 84, no. 7, pp. 3561–3568, 1998.

[17] E. Peiner, A. Schlachetzki, D. Krüger, "Doping profile analysis in Si by electrochemical capacitance-voltage measurements", *J. Electrochem. Soc.*, vol. 142, no. 2, pp. 576–580, 1995.

[18] A. Kimmerle, J. Greulich, A. Wolf, "Carrier-diffusion corrected J_0-analysis of charge carrier lifetime measurements for increased consistency", *Sol. Energy Mater. Sol. Cells*, vol. 142, pp. 116–122, 2015.

[19] F. Feldmann, B. Steinhauser, H. Nagel et al., "Industrial TOPCon solar cells realized by a PECVD tube process", *Proc. 37th EU PVSEC*, Lisbon, Portugal, 2020.

[20] R. Lago, L. Pérez, H. Kerp et al., "Screen printing metallization of boron emitters", *Prog. Photovolt.: Res. Appl.*, vol. 18, no. 1, pp. 20–27, 2010.

[21] F. D. Heinz, M. Breitwieser, P. Gundel et al., "Microscopic origin of the aluminium assisted spiking effects in n-type silicon solar cells", *Sol. Energy Mater. Sol. Cells*, vol. 131, pp. 105–109, 2014.

[22] S. Fritz, M. König, S. Riegel et al., "Formation of Ag/Al screen-printing contacts on B emitters", *IEEE J. Photovoltaics*, vol. 5, no. 1, pp. 145–151, 2015.

[23] S. Fritz, J. Engelhardt, S. Ebert et al., "Contacting boron emitters on n-type silicon solar cells with aluminium-free silver screen-printing pastes", *Phys. Status Solidi RRL*, vol. 10, no. 4, pp. 305–309, 2016.

[24] E. Cabrera, S. Olibet, J. Glatz-Reichenbach et al., "Experimental evidence of direct contact formation for the current transport in silver thick film metallized silicon emitters", *J. Appl. Phys.*, vol. 110, no. 11, p. 114511, 2011.

[25] S. Kontermann, A. Ruf, R. Preu et al., "Simulating the interface morphology of silver thick film contacts on n-type Si-(100) and Si-(111)", *Appl. Phys. Lett.*, vol. 101, no. 12, p. 121907, 2012.

[26] E. Lohmüller, S. Werner, B. Thaidigsmann et al., "The HIP–MWT+ solar cell concept on n-type silicon and metallization-induced voltage losses", *Proc. 29th EU PVSEC*, Amsterdam, The Netherlands, 2014, pp. 635–641.